The state dependence of the interaction of metastable rare gas atoms Rg*(ms 3 P 2 , 3 P 0) (Rg=Ne, Ar, Kr, Xe) with ground state sodium atoms

ARTICLE *in* ZEITSCHRIFT FÜR PHYSIK D · DECEMBER 1990

DOI: 10.1007/BF01437526 · Source: OAI

6 AUTHORS, INCLUDING:

Harald Morgner
University of Leipzig
131 PUBLICATIONS **1,765** CITATIONS

SEE PROFILE

Z. Phys. D – Atoms, Molecules and Clusters 16, 237–249 (1990)

Atoms, Molecules
Zeitschrift für Physik D and Clusters

The state dependence of the interaction of metastable rare gas atoms Rg*(ms $^3P_2$, $^3P_0$) (Rg = Ne, Ar, Kr, Xe) with ground state sodium atoms ⋆

S. Schohl [1], M.W. Müller [1], H.A.J. Meijer [1], M.-W. Ruf [1], H. Hotop [1], and H. Morgner [2]

[1] Fachbereich Physik, Universität Kaiserslautern, D-6750 Kaiserslautern, Federal Republic of Germany
[2] Institut für Experimentalphysik, Naturwissenschaftliche Fakultät, Universität Witten-Herdecke, D-5810 Witten, Federal Republic of Germany

Received 26 March 1990; final version 15 May 1990

Using crossed beams of metastable rare gas atoms Rg*(ms $^3P_2$, $^3P_0$) (Rg = Ne, Ar, Kr, Xe) and ground state sodium atoms Na($3s\ ^2S_{1/2}$), we have measured the energy spectra of electrons released in the respective Penning ionization processes at thermal collision energies. For Rg*($^3P_2$) + Na($3s$), the spectra are quite similar for the different rare gases, both in width and shape; they reflect attractive interactions in the entrance channel with well depths D_e^* [meV] decreasing slowly from Rg = Ne to Xe as follows: 676(18); 602(23); 565(26); 555(30). For Rg*($^3P_0$) + Na($3s$), the spectra vary strongly with the rare gas, indicating a change in the character of the interaction from van der Waals type attraction (Ne) to chemical binding for Kr and Xe with well depths D_e^* [meV] of: 51(19); 107(25); 432(30); 530(50). These findings are explained through model calculations of the respective potential curves, in which the exchange and the spin orbit interaction in the excited rare gas and the molecular interaction between the two valence s-electrons in terms of suitably chosen singlet and triplet potentials are taken into account. These calculations also explain qualitatively the experimental finding that the ratios q_2/q_0 of the ionization cross sections for Rg*($^3P_2$) + Na and Rg*($^3P_0$) + Na vary strongly with the rare gas from Ne to Xe as follows: 15.8(3.2); 2.6(4); 1.4(2); 1.6(4).

PACS: 31.20Pv; 31.50.+w; 31.70.−f; 34.20.−b; 34.50.Gb; 35.20.Gs; 82.40.Dm

1. Introduction

High resolution energy analysis of electrons resulting from ionizing thermal energy collisions of electronically excited atoms with atoms and molecules (Penning ionization) yields detailed information about the molecular interactions [1–12]. For most of these studies, metastable He*($2\,^3S$, $2\,^1S$) atoms have been used because of their high excitation energies ($\approx$20 eV), long lifetimes, ease of production and state selection, importance in discharges, and theoretical simplicity. The investigation of (quasi) one electron target atoms (H, D; alkali atoms A) is particularly important in connection with a thorough test of the theoretical description of the Penning process [5–8, 10–14]. Our group has recently reported detailed experimental studies of the electron spectra for He*($2\,^3S$, $2\,^1S$) + H, A [8, 10, 11, 13] along with quantum mechanical analyses [10, 11, 13] of part of the data, based on ab initio potentials [10, 11, 13, 14]. It was shown that the $^2\Sigma$-interaction of He*($2\,^3S$) atoms with $X = H$, A [8] is rather similar to the $^1\Sigma$-interaction of Li($2s$) atoms with X. In contrast, the He*($2\,^1S$) interaction with X is less strong [8, 11, 13, 14], but still appreciable (well depths 0.2–0.45 eV). In a continuing effort, to also characterize the interactions of the heavier metastable rare gas atoms Rg*($(m-1)p^5$ ms $^3P_2$, $^3P_0$) with a variety of other atoms [6, 7, 15], we have now investigated the systems Rg*(ms $^3P_2$, $^3P_0$) + Na($3s$) (Rg = Ne, Ar, Kr, Xe; m = 3–6). It is our aim to elucidate systematic trends in the behaviour of the different heavier metastable atoms interacting with a selected target atom X. Lorenzen et al. [6, 7] have previously observed an interesting, strongly different behaviour of Ne*($3s\ ^3P_2$) and Ne*($3s\ ^3P_0$) atoms in their interactions with X = H, D, Li, Na, K: the total ionization cross sections and potential well depths for Ne*($^3P_2$) + X are much larger then those for Ne*($^3P_0$) + X. It is therefore of particular interest to see how the dependence on the fine-structure state evolves from Ne to Xe for a selected target atom X.

Our studies are part of a broad effort to obtain a better understanding of spin-orbit effects in gas phase reactions, as previously discussed by Dagdigian and Campbell [16]. We also mention in this context recent work on chemical reactions involving state-selected metastable rare gas atoms, e.g. [17].

The paper is organized as follows: in Sect. 2, we describe the apparatus and experimental procedure. In Sect. 3.1, we present the electron energy spectra for

⋆ Dedicated to Prof. Dr. J.P. Toennies on the occasion of his 60th birthday

Rg*(ms $^3P_2$, $^3P_0$)+Na(3s) (Rg=Ne, Ar, Kr, Xe) and deduce the state dependence of the cross sections. The corresponding findings, especially a strong variation of the interaction of Rg*($^3P_0$)+Na in going from Ne to Xe, will be discussed and explained on the basis of model calculations of the potential energy curves for Rg*(ms)+Na, as described in Sect. 3.2. Using a semiclassical analysis and information from the model calculations, we deduce the well depths for the (attractive) potential curves of the Rg*(ms $^3P_2$, $^3P_0$)+Na(3s) systems in Sect. 3.3 and compare them with the well depths for the A(ms)+Na(3s) ($X^1\Sigma$) potentials of the analogous alkali atoms A(ms).

2. Experimental

The apparatus used for the present Penning ionization electron spectrometry (PIES) work is shown semi-schematically in Fig. 1. It consists of three separately pumped chambers: two source chambers and the reaction chamber, which houses a cylindrical mirror electron energy analyzer (CMA) within a three-layer μ-metal shielding (magnetic fields below 10^{-7} T). A well-collimated (1:70) metastable beam, originating from a DC cold cathode discharge source, crosses an equally well collimated effusive Na beam, coming from a two chamber oven, at right angle. The fluxes of the mixed metastable atom beams Rg*($^3P_2$, $^3P_0$) are in the range (10^{10}–10^{11})/s, and the Na(3s) target density is around $4\cdot10^9$ cm^{-3}.

Electrons originating from Rg*+Na ionization processes are detected with a CMA, whose axis is perpendicular to the plane spanned by the atomic beams. The CMA samples electrons ejected from the reaction center along a 54.7° half-angle cone around its symmetry axis. A lens system images the electrons from the reaction volume onto the entrance slit of the CMA operated at a constant pass energy of 8 eV with a nominal resolution of 40 meV (FWHM). The electrons are detected with a channel multiplier combined with fast counting electronics. The total efficiency of the system is estimated to be 1%. The spectra are accumulated with a multichannel scaler and are stored on our lab computer for further processing.

The electron energy dependent transmission of the electron spectrometer has been determined by means of photoionization of diffuse gas targets O_2 and NO by HeI_α photons. These photons were produced by a source in a fourth vacuum chamber (omitted from Fig. 1), opposite to the Na-oven chamber. The transmission was found to be constant within 5% over the relevant electron energy ranges.

Calibration of the energy scale has been performed by using PIES electrons from the reactions Rg*($^3P_{0,2}$) +NO → Rg+NO$^+$(X; v=0, 1), were always measured simultaneously with the Rg*+Na spectrum. The linearity of the spectrometer has been checked by measuring the He(I_α)+NO photoelectron spectrum in the range 0–12.5 eV and comparing it to literature values [18, 19]. We estimate the calibration error anywhere in the spectrum to be less than 8 meV. The effective energy resolution could be deduced from the measured widths of the NO-PIES calibration peaks, whose intrinsic widths had been accurately determined by comparison with photoelectron peaks. The effective resolution for all measurements presented here was 40–45 meV.

The background pressure of NO (about $3\cdot10^{-5}$ mbar in the reaction region), needed for the simultaneous energy calibration, had an unexpected, but very favourable side-effect: it decreased the overall shift of the electron energy scale, which amounted to (1–2) eV in the absence of NO, to stabilized values around 0.3 eV. Therefore we could increase the intervals, over which we accumulated single spectra, from about 10 to typically 40 minutes (thereby increasing the calibration accuracy), without deteriorating the effective resolution by potential drifts.

With the Na source running in the effusive regime, the normalized velocity density distribution $f_1(v_1)$ of the Na beam

$$f_1(v_1)=c_1\, v_1^2 \exp(-m_1\, v_1^2/2k_B\, T_1) \qquad (1)$$

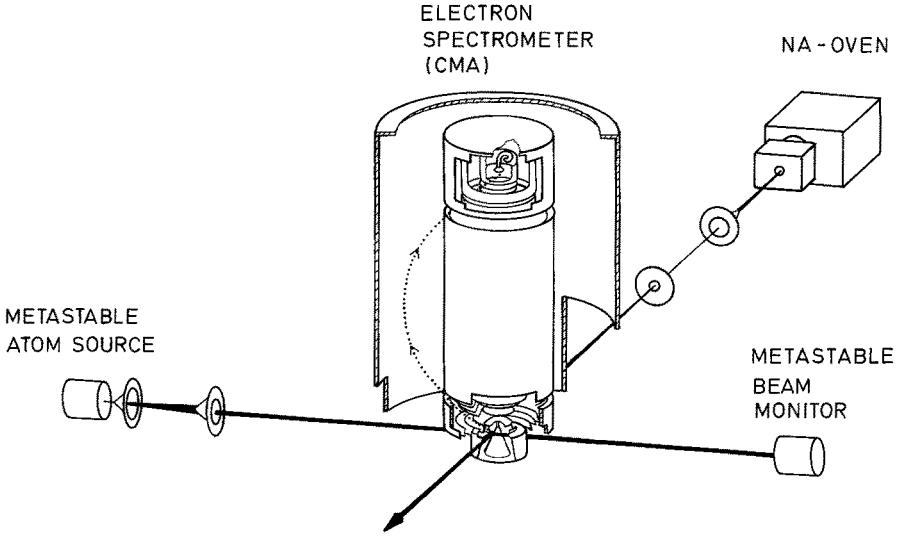

Fig. 1. Semi-schematic drawing of the apparatus used to study the energy spectra of electrons released in ionizing thermal energy collisions between metastable rare gas atoms and ground state sodium atoms. The symmetry axis of the cylindrical mirror electron energy analyzer (CMA) is perpendicular to the plane spanned by the two orthogonal atomic beams. The distance of the separately pumped metastable rare gas (sodium) atomic beam source to the reaction center is 185 mm (262 mm). The spectrometer is enclosed by a three-layer μ-metal shielding, which reduces the magnetic fields to values well below 10^{-7} T

Table 1. Velocity distribution parameters for the metastable rare gas projectile beams and the target sodium beam: m = average mass; T = beam temperature; u = flow velocity (see Eqs. (1) and (2)). With these parameters the collision energy distributions in Fig. 2 were calculated

Atom	m [amu]	T[K]	u [m/s]
Ne*($3s\ ^3P_{2,0}$)	20.18	28	790
Ar*($4s\ ^3P_{2,0}$)	39.95	28	560
Kr*($5s\ ^3P_{2,0}$)	83.80	28	390
Xe*($6s\ ^3P_{2,0}$)	131.30	28	310
Na($3s$)	22.99	723[a] 745[b]	0

[a] Temperature for Ar*, Kr*, Xe* data
[b] Temperature for Ne* data

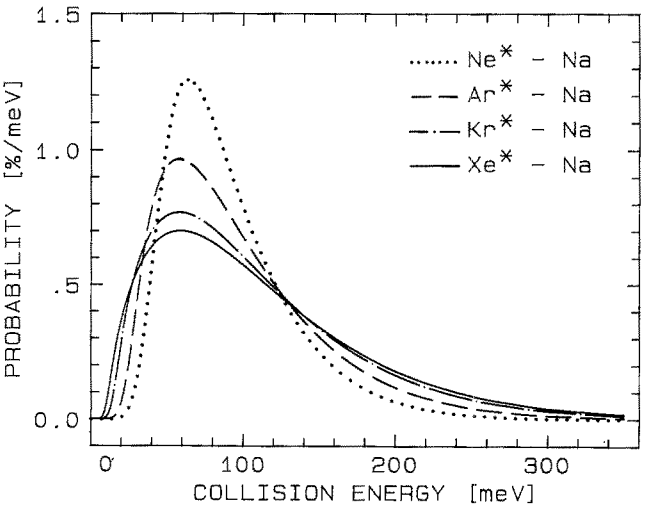

Fig. 2. Probability distributions $g_c(E_{rel})$ of the relative collision energies E_{rel} for the studied systems Rg*(ms $^3P_2$, $^3P_0$) + Na($3s$) (Rg = Ne, Ar, Kr, Xe; m = 3–6)

could be computed by using the temperature of the oven. Measurements on a similar oven [20] have shown this to be reliable.

The normalized velocity density distribution $f_2(v_2)$ of the metastable atoms has nozzle beam character, as described by

$$f_2(v_2) = c_2\, v_2^2 \exp(-m_2(v_2-u_2)^2/2k_B T_2). \tag{2}$$

The distributions for Ne* and Ar* metastable atoms have been measured by time of flight and laser Doppler-shift methods [21, 22]. For all measurements, the same discharge current (10 mA) and comparable gas pressures were used in the metastable atom source. The parameters u_2, T_2 for Kr* and Xe* were extrapolated from the results for Ne* and Ar*, as summarized in Table 1.

The total electron rate r due to reactions Na + Rg* can be written:

$$r = V n_1 n_2 \int_0^\infty \sigma(v_{rel}) f_c(v_{rel})\, \mathrm{d}v_{rel} \tag{3}$$

with V the interaction volume, n_1 and n_2 the total densities of Na and Rg*, respectively, $\sigma(v_{rel})$ the relative velocity dependent cross section and $f_c(v_{rel})$ the collision velocity distribution:

$$f_c(v_{rel}) = v_{rel} \int_0^\infty f_1(|\mathbf{v}_{rel}+\mathbf{v}_2|) f_2(v_2)\, \mathrm{d}v_2$$
$$= \int_0^\infty \int_0^\infty f_1(v_1) f_2(v_2)\, |\mathbf{v}_1-\mathbf{v}_2|\, \delta(v_{rel}-|\mathbf{v}_1-\mathbf{v}_2|)\, \mathrm{d}v_1\, \mathrm{d}v_2 \tag{4}$$

Using $E_{rel} = \frac{1}{2}\mu v_{rel}^2$ and $\mathrm{d}v_{rel} = \mathrm{d}E_{rel}/\mu v_{rel}$, one gets the collision energy distribution $g_c(E_{rel})$. This physically important distribution is shown in Fig. 2 for all four reactions.

In the case of Rg* = Ne, Kr we used a laser state selection method [15, 23], to obtain separate $^3P_2$- and $^3P_0$-spectra and relative $^3P_2$:$^3P_0$ cross sections. A multimode dye laser with narrow mode spacing (around 70 MHz), a bandwidth around 10 GHz, and a power of (100–200) mW excited a suitable Rg*(ms $^3P_2 \rightarrow$ mp, $J=1$) transition to simultaneously remove the Rg*(ms $^3P_2$) atoms and enhance the Rg*(ms $^3P_0$) flux in the counterpropagating Rg* beam.

As an example Fig. 3 shows Kr* + Na spectra with and without the state selecting laser (557.0 nm), pumping the Kr*($5s\ ^3P_2 \rightarrow 5p'[1/2]_1$) transition. The accompanying Kr* − NO spectrum (which will be discussed elsewhere in detail) allows us to keep track of the efficiency of the state selection process and to determine accurately the enhancement of the $^3P_0$ flux. From this increase, a relative $^3P_2$:$^3P_0$ flux $j_2/j_0 = 11.0 \pm 1.3$ in the mixed metastable beam can be calculated by using known Einstein coefficients for the decay of the laser-excited Kr*($5p'[1/2]_1$) level [23]. With this flux ratio, relative $^3P_2$:$^3P_0$ cross sections are calculated from the intensities of the energy-integrated electron spectra for $^3P_2$ and $^3P_0$. For details of this procedure, the reader is referred to earlier work [15, 23].

Application of analogous laser state selection to Ar* [17, 23] and Xe* [24] is desirable, but was not used in the present work. The Xe*($^3P_2$) and Xe($^3P_0$) spectra do not ovelap (see Fig. 6), and the Ar*($^3P_2$) and Ar*($^3P_0$) spectra could be deconvoluted on the basis of a reasonable extension of the Ar*($^3P_2$) spectrum into the energy range of the rather narrow Ar*($^3P_0$) spectrum (see Fig. 5). The $^3P_2$:$^3P_0$ cross section ratios for Ar* and Xe* are based on $^3P_2$:$^3P_0$ fluxes of $j_2/j_0 = 6.3 \pm 0.2$ for Ar*, measured previously [23] for a source of the same type, and $j_2/j_0 = 13 \pm 3$ for Xe*. The latter value was extrapolated graphically from the measured ratios j_2/j_0 for Ne*, Ar*, and Kr*, by using the empirical finding that a double-log plot of j_2/j_0 versus fine structure separation yields a straight line (see Fig. 4).

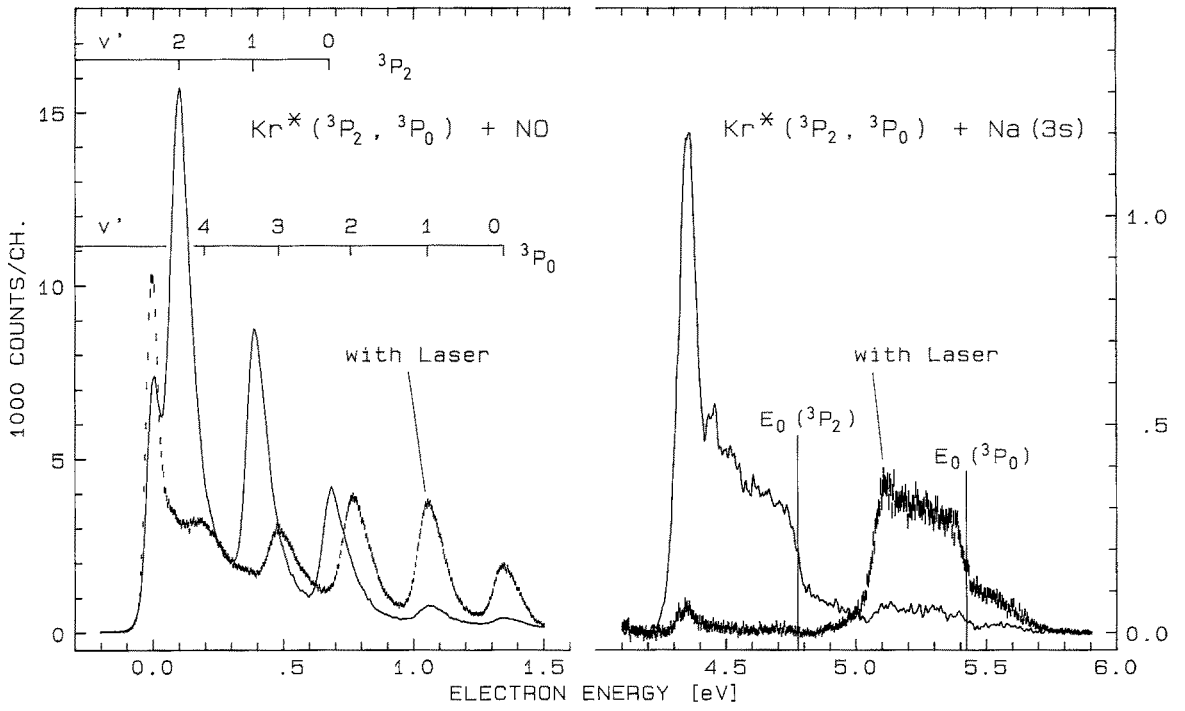

Fig. 3. Electron energy spectra due to ionizing collisions of metastable Kr* atoms with a mixed target, containing Na(3*s*) atoms and NO (X, $v''=0$) molecules. The smooth line represents the spectrum measured with a normal, mixed Kr*(5*s* $^3P_2$, $^3P_0$) beam ($^3P_2$: $^3P_0$ flux ratio 11 ± 1.3). The data points with error bars represent the data obtained with laser state-selection at $\lambda=557.0$ nm; the $^3P_2$ component is reduced to about 5% of its normal flux, and the $^3P_0$ component is correspondingly enhanced by cross-pumping from the $^3P_2$-level (fractional conversion 57.7% [23]), yielding almost pure $^3P_0$ spectra of Na(3*s*) and NO

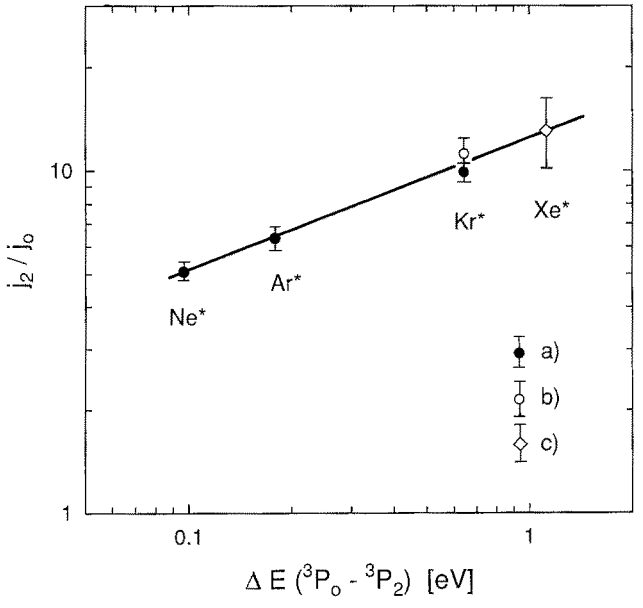

Fig. 4. Flux ratio j_2/j_0 of metastable rare gas atoms Rg*($^3P_2$), Rg*($^3P_0$), measured for our discharge source under typical conditions (current 10 mA, source gas temperature around 300 K) for Rg=Ne, Ar, Kr (results a): Ref. 23; b): present work). For Rg=Xe, a flux ratio $j_2/j_0=13\pm3$ is extrapolated (square labelled c)), as shown in the figure

3. Results and discussion

3.1. Electron energy spectra and state dependence of cross sections

The experimental results are shown in Figs. 3, 5–7. Figs. 3, 5, and 6 show the Kr*, Ar*, and Xe* spectra, respectively, on absolute electron energy scales, whereas in Fig. 7, the $^3P_2$ and $^3P_0$ spectra are plotted relative to the nominal energies $E_0(^3P_2)$ and $E_0(^3P_0)$, respectively (E_0=excitation energy of Rg* minus ionization energy of Na(3*s*)). The $^3P_2$ electron spectra are very similar for all four systems: they are dominated by a peak at electron energies $E_p<E_0$, typical for a system having an attractive excited state potential $V^*(R)$ corresponding to well depths of several tenths of an eV [1, 7, 8]. A secondary Airy-type maximum [3, 5–13] is observed, which gradually disappears from Ne* to Xe*; this behaviour reflects the combined effects of the decrease in the well depths and the increase in the reduced mass and in the number of contributing partial waves, when going from Ne* to Xe*. The high energy tail of the spectra ($E>E_0$), most clearly seen in the Xe data, is due to ionization at closer R range and reflects, in part, the attraction of the Rg+Na$^+$ exit channel potential.

In the Rg*($^3P_0$)–Na spectra, on the other hand, the shape changes dramatically from a structureless narrow

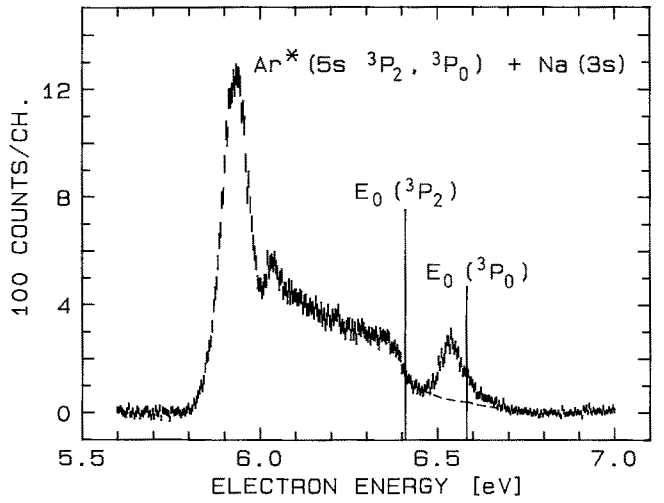

Fig. 5. Electron energy spectra due to ionizing collisions of a mixed metastable Ar*($4s$ $^3P_2$, $^3P_0$) beam ($^3P_2$: $^3P_0$ flux ratio about 6.3 [23]) with a crossed Na($3s$) beam. The dashed line in the range (6.4–6.7) eV indicates how the $^3P_2$-spectrum was extrapolated for the purpose of extracting the $^3P_0$-spectrum shown in Fig. 7. The vertical lines denote the positions of the respective nominal electron energies E_0 (difference between the Rg* excitation energy and the Na($3s$) ionization energy)

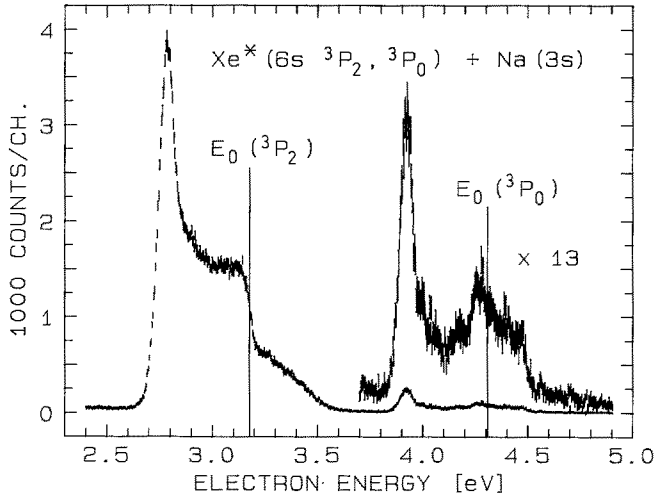

Fig. 6. Electron energy spectra due to ionizing collisions of a mixed metastable Xe*($6s$ $^3P_2$, $^3P_0$) beam ($^3P_2$: $^3P_0$ flux ratio about 13, see Fig. 4) with a crossed Na($3s$) beam. The fine-structure separation between the $^3P_2$ and $^3P_0$ level is sufficiently large ($E_0(^3P_0) - E_0(^3P_2) = 1.132$ eV) that the respective spectra do not overlap

peak close to the nominal energy for Ne* to a remarkably structured spectrum with a width similar to that of the $^3P_2$ spectrum for Xe*. These spectral changes for Rg*($^3P_0$) are accompanied by a decrease in the cross section ratio q_2/q_0 from above 10 for Ne* to values between 1 and 2 for Kr* and Xe* (see below). Model calculations of the adiabatic potential curves for Rg*(ms)+Na($3s$), based on attractive singlet and basically repulsive triplet valence electron interactions, will

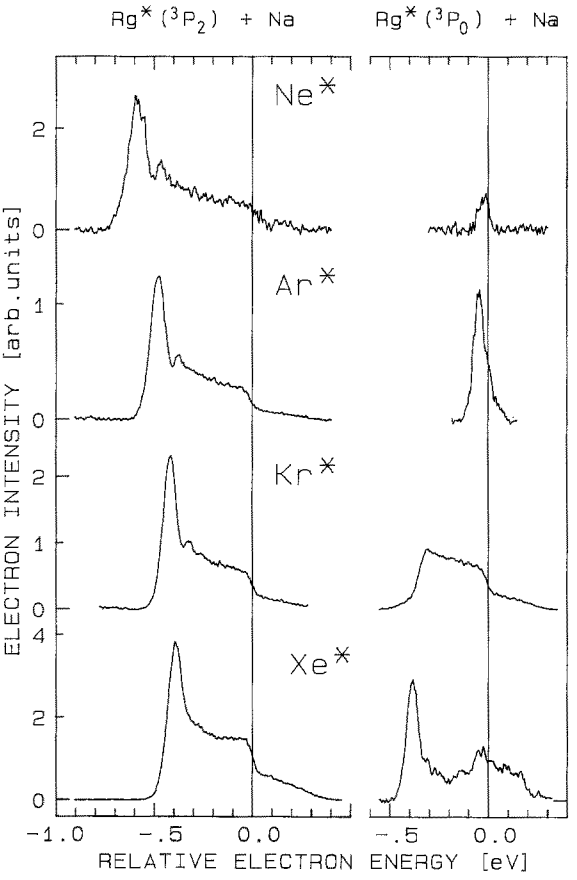

Fig. 7. Comparison of the electron energy spectra due to ionizing collisions of metastable rare gas atoms Rg*(ms $^3P_2$), Rg*(ms $^3P_0$) (Rg=Ne–Xe; $m=3-6$) with ground state sodium atoms Na($3s$) on a common relative energy scale $E-E_0$. For each rare gas, the two spectra are intensity-normalized such as to correspond to identical $^3P_2$ and $^3P_0$ fluxes. The intensity scales for the different rare gases cannot be directly compared in terms of relative cross sections

show (Sect. 3.2) that the experimental observations reflect the amount of singlet and triplet contributions of the valence electron interaction to the respective potential curves; for Rg*($^3P_0$)+Na($\Omega=1/2$) they vary strongly with the fine structure splitting of the rare gas core.

The areas under the spectra in Fig. 7 of each pair Rg*($^3P_2$) and Rg*($^3P_0$) are directly related to the respective total cross sections q_2 and q_0, i.e. the spectra are normalized such as to correspond to identical $^3P_2$ and $^3P_0$ fluxes. Table 2 shows the ratios q_2/q_0 together with the flux ratios j_2/j_0, upon which the evaluation is based (see also Fig. 4). For Ne*, the present ratio q_2/q_0 is in satisfactory agreement with the value of Lorenzen et al. [7], obtained with electron detection perpendicular to the plane of the crossed beams. For the heavier rare gases, the ratio q_2/q_0 is much smaller than for Ne with values approaching unity for Kr and Xe.

We could not determine absolute cross sections for the studied reactions, mainly because the metastable flux and the overall efficiency of the CMA were only roughly known. A mutual comparison of the cross sections for

Table 2. Ratios q_2/q_0 of the cross sections q_2 and q_0 for ionization in Rg*(ms $^3P_2$)+Na(3s) and Rg*(ms $^3P_0$)+Na(3s) collisions, respectively, and flux ratio j_2/j_0 of Rg*($^3P_2$) and Rg*($^3P_0$) atoms, which was used to determine q_2/q_0. The respective collision energy distributions, assumed to be identical for the two fine-structure levels of a given rare gas atom, are shown in Fig. 2

Rg*	j_2/j_0 [a]	q_2/q_0
Ne*	5.1 ± 0.3	15.8 ± 3.2 [b] 11.9 ± 2.4 [c]
Ar*	6.3 ± 0.5	2.6 ± 0.4 [b]
Kr*	11.0 ± 1.3	1.4 ± 0.2 [b]
Xe*	$13\ \pm3$	1.6 ± 0.4 [b]

[a] See also Fig. 4 and text; the error limits include the uncertainties in the laser optical determination of j_2/j_0 due to the limited precision of the relevant Einstein factors ($\leqq 5\%$, see Ref. 23)

[b] Results of the present work; the data correspond to a weighted average over the range $35° \leqq \Theta \leqq 145°$ of electron emission angles Θ (with respect to the relative collision velocity), see also Ref. 13. If the electron energy-integrated, Θ-dependent cross sections $\frac{dq}{d\Omega}(\Theta)$ are isotropic (as expected for strongly attractive systems [2, 3], such as Rg*($^3P_2$)+Na and Kr*($^3P_0$), Xe*($^3P_0$)+Na) or an ungerade function with respect to $\Theta=90°$, spectral areas obtained at $\Theta=90°$ (Ref. 7) or with an angular average as in the present work reflect the total cross sections q. In other cases, our setup is expected to yield results closer to the total cross sections than setups with electron detection at $\Theta=90°$

[c] Ref. 7; electron detection perpendicular to relative velocity

the different rare gases involves the knowledge of their relative fluxes; although we monitored the metastable flux by electron emission from a (gas-covered) stainless steel plate, the corresponding detector currents are not significant, because the respective electron emission coefficients γ were not known. We mention, however, that more recently, we have developed an accurate method to determine γ for metastable rare gas atoms [25].

The model calculations of the Rg*+Na interactions, to be described in the next section, will provide a qualitative explanation for the strong variation of q_2/q_0 with Rg* (Rg=Ne−Xe).

3.2. Model calculations for the excited rare gas-sodium potentials and discussion of the ionization-favoured, distance dependent spin configurations

The interaction potentials between the excited rare gases Rg*($(m-1)\,p^5$ ms) and an alkali atom A(ns) (here A(ns)=Na(3s)) shall be described by a simple model, which is sufficient for the purpose of this paper. We exploit the well-known fact that excited rare gas atoms display a chemical behaviour which is very much like the behaviour of the analogous alkali atom following in the periodic table [3, 7, 26–28]. In our context this means that we start with the known alkali-alkali interaction potential and add merely the fine-structure produced by the nonisotropic ionic core of the excited rare gas atom.

Four angular momenta are defined in our model:

s_c: spin of the rare gas core $Rg^+((m-1)\,p^5)$
l_c: orbital angular momentum of $Rg^+((m-1)\,p^5)$
s_v: spin of the valence electron of the rare gas
s_A: spin of the alkali electron

These angular momenta can be coupled in several ways to give a total angular momentum J. Each way of coupling defines a different basis set.

We denote the angular momentum of a subsystem by giving the two composing momenta in parenthesis. With this prescription we can define unambiguously our chosen basis sets:

Basis I: $S_{Rg}(s_c, s_v)$ total spin of rare gas
$J_{Rg}(S_{Rg}, l_c)$ total angular momentum of rare gas
$J(J_{Rg}, s_A)$

Basis II: $k_c(l_c, s_c)$ total angular momentum of ionic rare gas core
$J_{Rg}(k_c, s_v)$
$J(J_{Rg}, s_A)$

Basis III: $k_c(l_c, s_c)$
$S_V(s_A, s_v)$ spin of the two chemically active valence electrons
$J(S_V, k_c)$

Basis IV: $S_{PI}(s_c, s_A)$ spin that controls Penning ionization
$S(S_{PI}, s_v)$ total spin of the whole system
$J(S, l_c)$

Three types of interaction are included in our model:

i) the exchange matrix element within the excited rare gas. It depends solely on the value of S_{Rg}. Thus, this interaction is diagonal in bases I and IV. The values are

$$+K \quad \text{for } S_{Rg}=0 \quad \text{and} \quad -K \quad \text{for } S_{Rg}=1;$$

ii) the spin orbit interaction of the ionic rare gas core. It is diagonal in bases II and III, depends only on k_c, and has the values

$$\zeta_p \quad \text{for } k_c=1/2 \quad \text{and} \quad -\tfrac{1}{2}\zeta_p \quad \text{for } k_c=3/2;$$

iii) the chemical interaction operator involving the valence electrons, i.e. ms of the rare gas and ns of the alkali. Among the given angular momenta it depends only on $S_V(s_A, s_v)$. This interaction is diagonal in basis III. We define (for arbitrary values of k_c and J)

$$\langle S_V|\hat{V}|S_V\rangle = \begin{cases} V_s & \text{for } S_V=0 \\ V_t & \text{for } S_V=1 \end{cases}$$

Further interactions, e.g. the interaction between the ionic core of the rare gas and the alkali, are omitted in order to keep the model simple. We will observe that the model suffices to explain the essential experimental findings.

The quantities $V_s(R)$ and $V_t(R)$ are to be identified with the attractive singlet and the repulsive triplet potential of the corresponding alkali-alkali system. For our

model calculations we have chosen the analytical potentials:

$$V_s(R) = D_e^s[e^{2y}(1 - c_3 y^3 - c_4 y^4) - 2e^y], \quad (5)$$
where $y = \beta^s(1 - R/R_e^s)$

and

$$V_t(R) = D_e^t[e^{2y} - 2e^y], \quad (6)$$
where $y = \beta^t(1 - R/R_e^t)$.

With the numerical values of the parameters

$$D_e^s = 739 \text{ meV};\ R_e^s = 5.854 a_0;\ \beta^s = 2.657;$$
$$c_3 = 0.317;\ c_4 = -0.186 \quad (5a)$$
$$D_e^t = 20.5 \text{ meV};\ R_e^t = 9.885 a_0;\ \beta^t = 3.898 \quad (6a)$$

the given forms fit accurate ab initio potentials [29] of the sodium dimer $Na_2(X^1\Sigma)$ and $Na_2(a^3\Sigma)$ very well in the R range of interest (3–$15 a_0$).

In order to elucidate clearly the differences between the molecular potentials for Rg*(ms)+Na(3s), as induced by the changes in the atomic parameters for the considered Rg*(ms) atoms (i.e. mainly by the strongly varying spin-orbit interaction ζ_p), we choose the same pair of singlet and triplet potentials V_s, V_t (as given by equations (5), (6), (5a) (6a)) for the computation of all the Rg*(ms)+Na(3s) systems. In view of the similarity in the chemical properties of the Na(3s) and Ne*(3s) atoms [26–28], the chosen pair V_s, V_t is best suited for the description of the Ne*(3s)+Na(3s) system. For the heavier rare gas atoms, the calculated Rg*(ms)+Na(3s) potentials will be less accurate in a quantitative sense, but they will fully reflect the important qualitative aspects (note that the well depths of the A(ms)+Na(3s) $(X^1\Sigma)$ potentials, as listed in Table 5, decrease by only 18% from Na_2 to CsNa).

Using the values for ζ_p and K listed in Table 3, and setting $V_s = V_t = 0$ in our program, we have reproduced the energy spacings between the four levels of the atomic configuration $(m-1)p^5$ ms for Ne, Ar, and Kr within one meV; for Xe, the positions of the $^1P_1$ and $^3P_1$ levels relative to the properly spaced $^3P_0$ and $^3P_2$ levels are off by -29 meV and $+29$ meV, respectively.

Within our model, the different behaviour of the excited rare gases in reactions with sodium is caused by the ratio between the internal rare gas matrix elements ζ_p and K and the well depths of V_s and the splitting $V_t - V_s$.

Table 3. Spin orbit interaction parameter ζ_p and exchange matrix element K for the excited rare gas atoms Rg*$((m-1)p^5$ ms)

Rg*	ζ_p [meV]	K [meV]
Ne*$(2p^5 3s)$	64.2	92.2
Ar*$(3p^5 4s)$	116.5	89.7
Kr*$(4p^5 5s)$	431.5	99.1
Xe*$(5p^5 6s)$	754.6	122.0

After setting up this model the computation of the Rg*$((m-1)p^5)$ ms)+A(ns) potential curves is standard: all interaction matrices are written down in the basis that makes them diagonal, transformed to one common basis, added and the resulting matrix is diagonalized.

We note that our model does not incorporate any interaction that is sensitive to the orientation with respect to the internuclear axis. Thus, total J is always a good quantum number. This has the consequence that eigenstates with different $\Omega = J_z$ values are identical within the model.

Thus, the potential curves, plotted in Fig. 8, may be understood as the subset of the seven $\Omega = 1/2$ potentials, but the respective $\Omega > 1/2$ potentials are degenerate with these.

In the present work, we are most interested in the $\Omega = 1/2$ subgroup of the Rg*(ms)+Na(3s) potential curves; among them the Rg*(ms $^3P_0$)+Na(3s) potential (labelled "e" in Fig. 8) and the most strongly attractive Rg*(ms $^3P_2$)+Na(3s) potential (curve "a"), which has $^2\Sigma_{1/2}$ character at smaller R, are found. Within the electron exchange model for Penning ionization [30, 31], one expects the latter potential to be the major contributor to ionization in Rg*(ms $^3P_2$)+Na(3s) collisions, as discussed previously for Ne*(3s $^3P_2$)+H, Li, Na, K [6, 7]. Its calculated potential well depth $D_e^*(a)$ reaches about 94% of the well depth D_e^s for the singlet potential V_s (see Table 4). The increase of the energy separation $E_0 - E_p$ in the Rg*($^3P_0$)+Na electron energy distribution in going from Rg=Ne to Rg=Xe is fully compatible with the rise of the respective well depths in the calculated Rg*(ms $^3P_0$)+Na(3s) potentials; the rise reflects the increasing admixture of the $^1\Sigma$-interaction between the valence electrons. In Table 4, we summarize some of the important results of the model calculations, namely the well depths $D_e^*(a)$, $D_e^*(e)$ of the potential curves "a" and "e" in Fig. 8 and the ratio $R_e^*(e)/R_e^*(a)$ of the respective equilibrium distances. These numbers clearly express the change in the character of the Rg*(ms $^3P_0$)+Na(3s) potential from van der Waals type attraction for Rg=Ne (predominantly containing the triplet valence electron interaction) to chemical binding (singlet valence electron interaction) for Kr and especially for Xe.

Another interesting result, concerning the ratio q_2/q_0 of the $^3P_2$ and $^3P_0$ ionization cross sections, can be evaluated from our calculation as well. We transform the eigenvectors into basis IV, which specifies the total spin S. It is well known that Penning ionization out of a quartet state (i.e. $S = 3/2$) cannot occur since the final state $Rg(^1S_0) + Na^+(^1S_0) + e^-$ is necessarily a doublet state. Thus, the summed weight w_d of all doublet basis states (i.e. $S = \frac{1}{2}$) can be understood as a relative, upper-bound measure for the probability that Penning ionization occurs. In Fig. 9A–D we have plotted the doublet contribution w_d in the various molecular states. The particularly large value of q_2/q_0 for Neon is readily understood as a consequence of the low doublet contribution ($w_d \approx 10\%$) to the Ne*($^3P_0$)+Na molecular state (state "e"), which leads to a low value of q_0; note that the doublet content of the state "a", responsible for ionization in Rg*($^3P_2$)+Na, is practically 100% for all Rg*

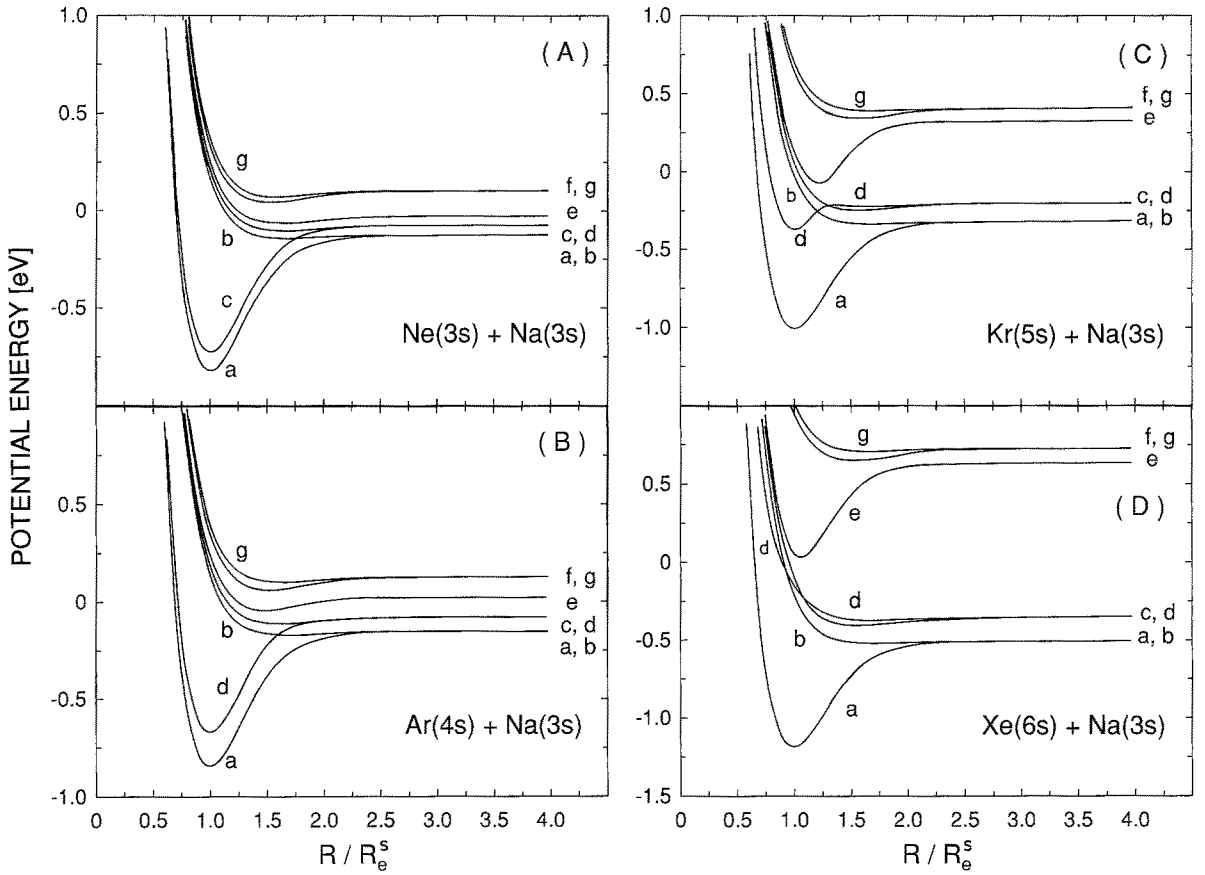

Fig. 8A–D. Results of model calculations for the Rg*(ms)+Na(3s) potential energy curves, as described in the text. **A**): Ne*(3s)-+Na(3s); **B**): Ar*(4s)+Na(3s); **C**): Kr*(5s)+Na(3s); **D**): Xe*(6s)-+Na(3s). With increasing fine-structure splitting of the rare gas atom, the potential curve labelled "*e*", which represents the Rg*(ms $^3P_0$)+Na(3s) interaction, becomes more attractive; for Rg=Xe, the well depth of curve "*e*" amounts to 91% of the well depth of curve "*a*", which is mainly responsible for ionization in the Rg*($^3P_2$)+Na(3s) system. Note that for reasons of simplicity, identical input potentials for the singlet and triplet interaction between the two valence electrons have been used for all the four rare gases (see Eqs. (5), (5a), (6), (6a))

Table 4. Selected results of the model calculations for the potential curves "*a*" and "*e*" of the Rg*(ms)+Na(3s) molecules (see Fig. 8)

Mol. System	$D_e^*(a)$ [meV]	$D_e^*(e)$ [meV]	$R_e^*(e)/R_e^*(a)$
Ne*(3s)+Na(3s)	698	37	1.62
Ar*(4s)+Na(3s)	699	73	1.50
Kr*(5s)+Na(3s)	695	410	1.22
Xe*(6s)+Na(3s)	685	607	1.06
	D_e^s [meV]	D_e^t [meV]	R_e^t/R_e^s
Na(3s)+Na(3s)[a]	739	20.5	1.689

[a] Ab initio results [29] for the $Na_2(X^1\Sigma)$, $Na_2(a^3\Sigma)$ potentials, which were used as input for V_s, V_t in the model calculations

at the relevant distances (see Fig. 9). Ar*+Na is an intermediate case with $w_d(e)\approx 40\%$, whereas for Kr*+Na and Xe*+Na, $w_d(e)$ is around 90% in the relevant R range.

More insight can be obtained by projecting out the states with $S_{PI}=0$. S_{PI} is the spin that controls Penning ionization according to the exchange mechanism. As long as only covalent configurations contribute to the molecular states, $S_{PI}=0$ is a strict criterion for Penning ionization to occur. The criterion $S=\frac{1}{2}$ (i.e. non-quartet states) provides an upper bound for the presence of ionization-favoured spin configurations within the considered molecular state. Since the molecular interaction in the alkali-Na(3s) $X^1\Sigma$ ground states has predominantly covalent character [29], inspection of the summed weights w_{PI} for ionization-favoured states with $S_{PI}=0$ promises to yield interesting additional information beyond that contained in Fig. 9. In Fig. 10, we summarize the results for the distance dependent weights w_{PI} for all the Rg*(ms)+Na(3s) systems.

As is clear from the results in Fig. 9, the state "*b*" ($w_d(b)=0$ for all R) possesses $w_{PI}(b)=0$ at all R; the state "*a*" always starts with a value $w_{PI}(a)=0.626$ (which is smaller than $w_d(a)=0{,}834$) at large R, but reaches values $w_{PI}(a)$ close to 1 for $R/R_e^s\lesssim 1.5$. Therefore, one expects that about half of the Rg*(ms $^3P_2$)+Na collisions proceed in ionization-favoured spin configurations. The state "*e*", describing Rg*(ms $^3P_0$)+Na(3s), always starts out with $w_{PI}(e)=1/4$ at large R (where $w_d(e)=1/3$). For Rg=Ne, $w_{PI}(e)$ strongly decreases for $R/R_e^s\lesssim 2$ and is close zero for $R/R_e^s\lesssim 1.3$; for Rg=Ar, $w_{PI}(e)$ first rises towards lower R, reaches a maximum $w_{PI}(a)\approx 0.33$ at $R/R_e^s\approx 1.8$, decreases strongly for $R/R_e^s\lesssim 1.7$, and is close to zero for $R/R_e^s\lesssim 1.2$. For Kr and Xe, $w_{PI}(e)$ rises strong-

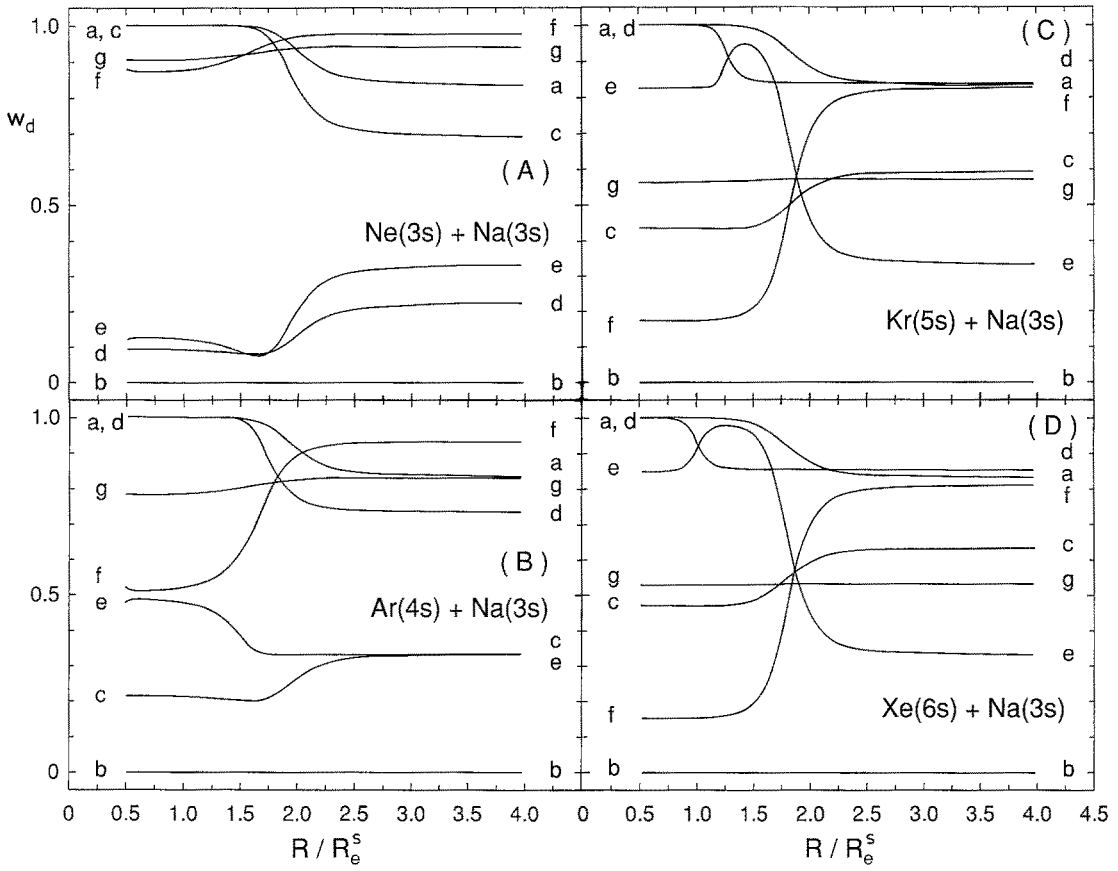

Fig. 9A–D. Results of model calculations for the summed weight w_d of doublet basis states as a function of reduced internuclear distance R/R_e^s ($R_e^s = 5.854 a_0$, see Eq. (5a)). Since the autoionization of quartet states is spin-forbidden, the quantity w_d can be understood as a relative upper-bound measure for the probability that ionization occurs. **A**): Ne*(3*s*)+Na(3*s*); **B**): Ar*(4*s*)+Na(3*s*); **C**): Kr*(5*s*)+Na(3*s*); **D**): Xe*(6*s*)+Na(3*s*)

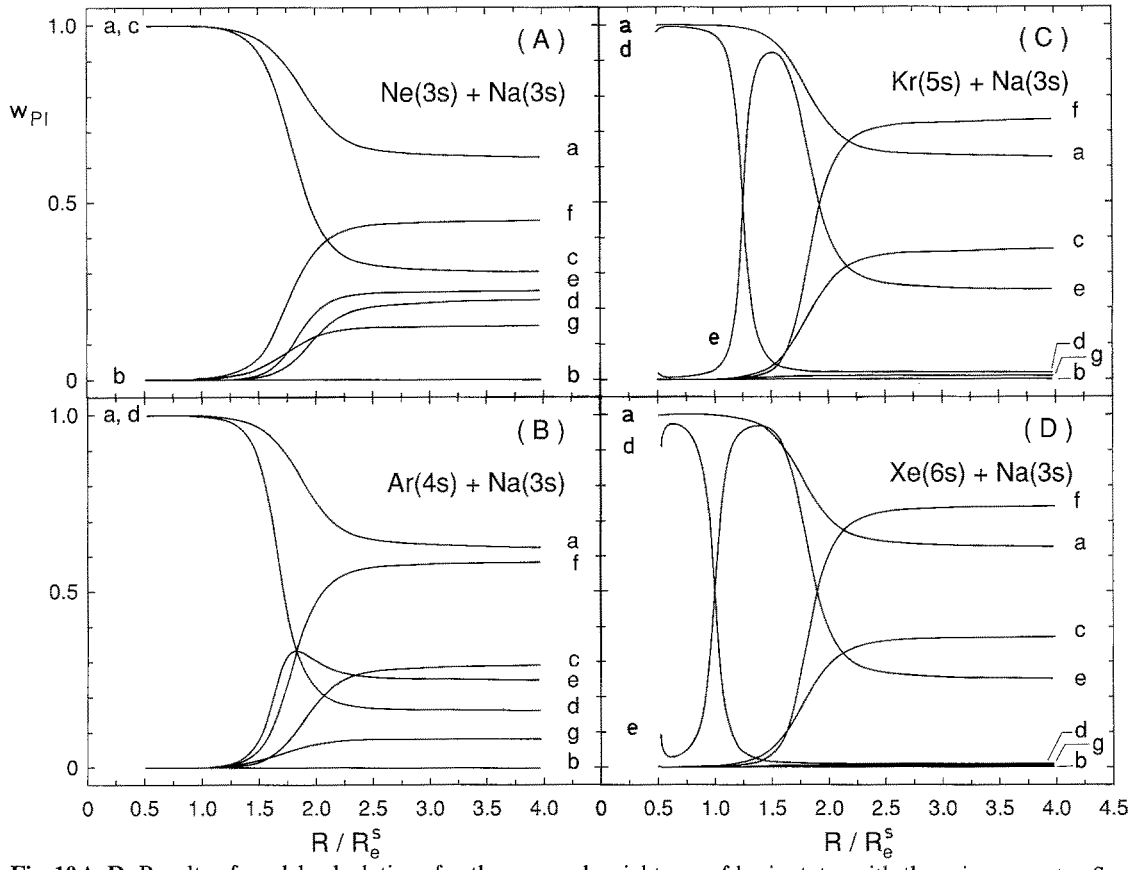

Fig. 10A–D. Results of model calculations for the summed weight w_{PI} of basis states with the spin symmetry $S_{PI}=0$, which is favourable for Penning ionization (see text). **A**): Ne*(3*s*)+Na(3*s*); **B**): Ar*(4*s*)+Na(3*s*); **C**): Kr*(5*s*)+Na(3*s*); **D**): Xe*(6*s*)+Na(3*s*)

ly for $R/R_e^s \lesssim 2$, reaching values above 0.9 for R/R_e^s around 1.5(Kr) and 1.4(Xe) and followed by a sharp decline towards values below 0.1; for Xe, this drop occurs at smaller distances (shift in R/R_e^s about 0.25).

In summary, the calculated potentials (Fig. 8) and the R-dependent weights w_{PI} (Fig. 10) lead to the following statements and predictions:

i) the shapes of the electron spectra for Rg*(ms $^3P_2$)+Na(3s) should be rather similar for all the rare gases with total energy widths in the range 0.5–1.0 eV.

ii) the total ionization cross sections q_2 should not differ much between the rare gases in view of the similarities of the relevant potentials "a" and weights $w_{PI}(a)$.

iii) the electron energy distributions for Rg*(ms $^3P_0$)+Na(3s) should be quite narrow for Rg=Ne, Ar, but much wider for Kr and Xe.

iv) the total ionization cross sections q_0 strongly rise from Rg=Ne to Rg=Kr and are rather similar for Kr and Xe.

All these statements are compatible with the experimental findings for the electron spectra and for the cross section ratios q_2/q_0.

In addition, the peculiar shape of the energy distribution for Kr*(5s $^3P_0$)+Na(3s), which does not exhibit a clear peak at low energies, may find its explanation through the special R-dependence of $w_{PI}(e)$ and thereby the autoionization width function $\Gamma(R)$ for this system in the region, where the potential "e" goes through its minimum. It is well known that the slope of $\Gamma(R)$ for distances around R_e^* has a significant influence on the appearance of the Airy-type structure at lower electron energies (see, e.g., [10, 13]). It should be noted, however, that the high energy tail of the Kr*(5s $^3P_0$)+Na(3s) electron spectrum most likely indicates a significant occurrence of ionizing transitions at closer distances (where the difference potential $V^*(R)-V^+(R)$ is larger than the asymptotic energy difference $E_0=V^*(\infty)-V^+(\infty)$), i.e. in a range of distances, where w_{PI} is close to zero. This discrepancy is also present, although to a lesser degree, for the system Xe*(6s $^3P_0$)+Na(3s); the electron spectrum of this system also shows an extended high energy tail, but exhibits – in contrast to Kr*($^3P_0$)+Na – usual structure around E_0 and a prominent low energy peak. Detailed analyses of the various electron distributions, which we plan to perform in the near future, are needed to clarify the remaining questions.

3.3. *Evaluation of the well depths for the Rg*(ms $^3P_2$, $^3P_0$)+Na(3s) potential curves and comparison with the A(ms)+Na(3s) interactions*

As demonstrated in previous work [7, 8, 11, 13, 32], a rather simple semiclassical analysis of the low energy edge of the Penning electron energy spectra for attractive systems can yield accurate values for the well depths of the respective entrance channel potentials $V^*(R)$. In this section, we basically proceed along the lines of [8], but implement a simple modification of the evaluation procedure, which takes into account the variation of the ionic exit channel potentials $V^+(R)$ in the R range

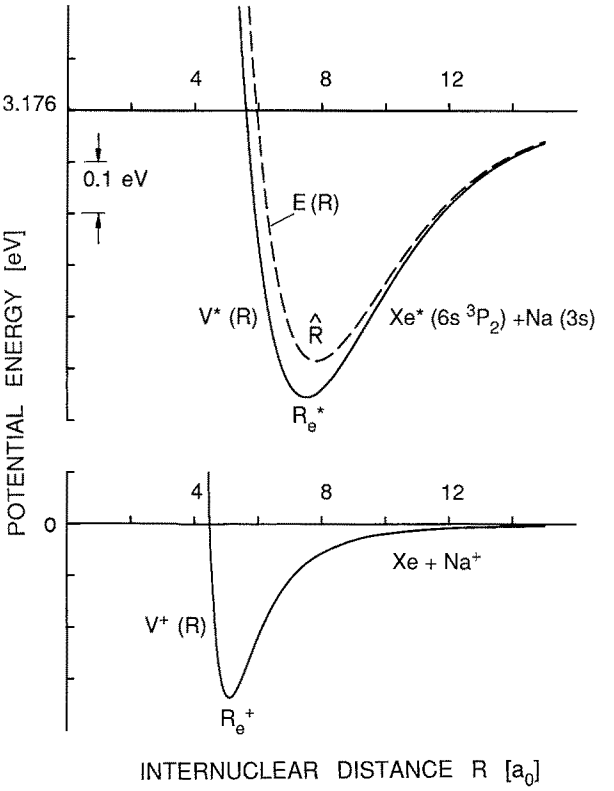

Fig. 11. Entrance channel potential $V^*(R)$, ionic exit channel potential $V^+(R)$, and difference potential $E(R)=V^*(R)-V^+(R)$, as relevant for the system Xe*(6s $^3P_2$)+Na(3s). The potential $V^*(R)$ corresponds to the model potential curve "a" in Fig. 8D) with adjusted well depth D_e^* and equilibrium distance R_e^*, as given in Table 4. The ionic potential was provided by Toennies [35], as obtained in a model analysis of the Xe–Na^+ interaction (see Ref. 34 for the procedure). Note that the position $\hat{R}$ of the minimum of the difference potential is shifted to larger distances relative to R_e^* due to the influence of the attractive ionic potential

around the position R_e^* of the minimum of $V^*(R)$. This modification is necessary since – contrast to the situation for He* collisions [8], for which the ionic He+A^+ potentials are nearly constant for R around R_e^* – the ionic potentials Rg+A^+ for Rg=Ar, Kr, Xe show a non-negligible variation around R_e^*.

To illustrate the problem, we show in Fig. 11 potentials $V^*(R)$ and $V^+(R)$ as well as the local electron energy function $E(R)$ (given by the difference potential [1–8, 32])

$$E(R)=V^*(R)-V^+(R), \tag{7}$$

which are representative for the case of Xe*($^3P_2$)+Na collisions (the potential $V^*(R)$ corresponds to curve "a" in Fig. 8D with adjusted D_e^* and R_e^*). One observes that the position $\hat{R}$ of the minimum of the difference potential is at a somewhat larger distance than the position R_e^* of the minimum of $V^*(R)$ due to the variation of $V^+(R)$ in this R range. This complicates the evaluation of the well depth $D_e^*=V^*(\infty)-V^*(R_e^*)$ from the low energy edge E_* of the electron spectrum (i.e. the energy position, where the electron distribution $P(E)$ has dropped to 43.8% of its peak value [7, 8, 32]), which is closely related

to the minimum of the difference potential $E(\hat{R})$ [8]; as in [8], we use in the further evaluation the equation

$$E_* = E(\hat{R}) \equiv V^*(\hat{R}) - V^+(\hat{R}). \tag{8}$$

It is expected that this approximation introduces uncertainties in D_e^* below 10 meV [8]. In cases, for which $\hat{R}$ agrees with R_e^*, one obtains [8]

$$E_* = E(\hat{R}) = E(R_e^*) = V^*(\infty) - D_e^* - V^+(R_e^*) \tag{9}$$

and with $V^*(\infty) - V^+(\infty) = E_0 =$ nominal energy

$$D_e^* = E_0 - E_* + V^+(\infty) - V^+(R_e^*). \tag{9a}$$

For the present systems, these equations are of sufficient accuracy for Rg* = Ne.

The modification consists of a simple estimate of the difference $\Delta R = \hat{R} - R_e^*$, based on analytical, known expressions for the description of $V^*(R)$ and $V^+(R)$ in the range around R_e^* and $\hat{R}$. We set

$$V^*(R) = V^*(R_e^*) + (f/2)(R - R_e^*)^2 \tag{10}$$

and use for f the values of the corresponding alkali + Na potentials. We describe $V^+(R)$ by the long range polarization potential

$$V^+(R) = -c_p/R^4, \quad c_p = \alpha e^2/8\pi\varepsilon_0 \tag{11}$$

using the well-known polarizabilities α of the ground state rare gas atoms [33]. The minimum of the difference potential, based on (10) and (11), is found to lie at the distance

$$\hat{R} = [4c_p/f(\hat{R} - R_e^*)]^{1/5}. \tag{12}$$

Therefore, one can determine $\Delta R = \hat{R} - R_e^*$ by solving

$$\Delta R(\Delta R + R_e^*)^5 - 4c_p/f = 0. \tag{12a}$$

Using (10) in (8), one obtains for the well depth D_e^*

$$D_e^* = E_0 - E_* + (f/2)\Delta R^2 + V^+(\infty) - V^+(R_e^* + \Delta R). \tag{13}$$

In (13), the quantity $(f/2)\Delta R^2 - V^+(R_e^* + \Delta R)$ replaces $-V^+(R_e^*)$ in the less accurate formula (9a). For all the systems discussed in this paper, ΔR is positive. Since $(f/2)\Delta R^2$ increases and $-V^+(R_e^* + \Delta R)$ decreases with rising ΔR (i.e. from Ne to Xe), the use of (13) instead of (9a) only yields rather small changes in the values derived for D_e^*.

In order to apply (13), we proceed as follows: E_* is taken from experiment and corresponds to the resolution-corrected value for the 44% low energy edge of the spectra. R_e^*, the most important unknown parameter, is estimated for Rg*($^3P_2$) + Na from the R_e values for the corresponding A + Na($X\,^1\Sigma$) potentials (see Table 5), increased by (0.2–0.3) a_0 to account for the somewhat smaller attraction of the Rg*($^3P_2$) + Na systems. A corresponding choice has been used previously [8] to estimate R_e^*[He*($2\,^3S$) + $A(^2\Sigma)$] from R_e[Li + $A(^1\Sigma)$] and corroborated more recently by accurate ab initio calculations for He*($2\,^3S$) + Li, Na [11, 13, 14]. For Rg*($^3P_0$) + Na, the estimates of R_e^* are based mainly on the results of the model calculations in Sect. 3.2, which yield $R_e^*[^3P_0 + \mathrm{Na}]$ in units of $R_e^*[^3P_0 + \mathrm{Na}]$ (only for Ne*($^3P_0$) + Na, R_e^* can be simply taken as R_e[Na + Na($a\,^3\Sigma$)]).

The curvatures f were estimated on the basis of the simple relation $fR_e/D_e = 2.15\,a_0^{-1}$ from the known R_e/D_e values for the alkali-Na($X\,^1\Sigma$) potentials (see Table 5); this relation was found to describe the curvatures f of the (Li, Na, K) + Na($X\,^1\Sigma$) potentials within 2%. The ΔR values were calculated from (12a), using the estimated or known numbers for R_e^*, f, and c_p. In the evaluation of D_e^* for Ne*($^3P_0$), Ar*($^3P_0$) + Na, the simpler formula (9a) was used, since the corresponding R_e^* are rather large and uncertain.

The ionic exit channel potentials are taken from recent work by Toennies et al. [34, 35] and are shown in Fig. 12, where $V^+(\infty) = 0$.

Table 5 summarizes the relevant potential parameters, the experimental results for E_*, and the final numbers for D_e^*. For Rg*($^3P_2$) + Na($3s$), the well depths slowly decrease from Ne* to Xe*; for all the rare gases, the D_e^* value is close to 90% of the well depth D_e for the analogous alkali-Na($3s$)($X\,^1\Sigma$) system. This behaviour is compatible with the results of the model calculations for the attractive potentials "a" (see Fig. 8 and Table 4). For Rg*($^3P_0$) + Na($3s$), on the other hand, the well depths increase strongly from Ne* to Xe*, especially from Ar*($^3P_0$) + Na($3s$) to Kr*($^3P_0$) + Na($3s$), for reasons discussed in Sect. 3.2.

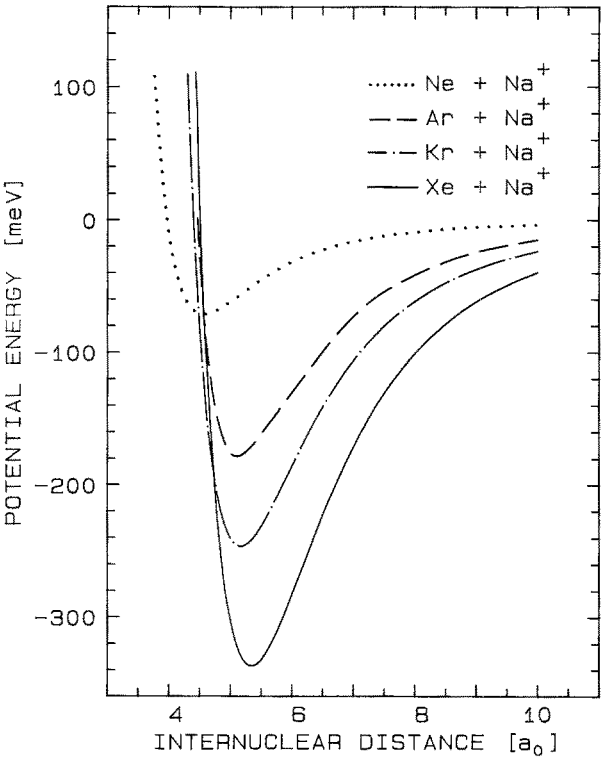

Fig. 12. Potential curves $V^+(R)$ for the Rg–Na$^+$ systems (Rg = Ne–Xe), used in the evaluation of the electron spectra. They were calculated by Ahlrichs et al. [34] for Rg = Ne, Ar and by Toennies [35] for Rg = Kr, Xe

Table 5. Potential data for $A(\mathrm{ms})+\mathrm{Na}(3s)$ systems and well depth evaluation for $\mathrm{Rg}^*(\mathrm{ms}\ ^3P_2,\ ^3P_0)+\mathrm{Na}(3s)$ potentials from low energy edge E_* in the Penning electron spectra (see text)

$A(\mathrm{ms})+\mathrm{Na}(3s)$		Na(3s)	K(4s)	Rb(5s)	Cs(6s)
$R_e(X\,^1\Sigma)$	[a_0]	5.818[a,b]	6.608[d]	6.86[e]	7.275[f]
$D_e(X\,^1\Sigma)$	[meV]	746.7(2)[b]	654.0(1)[d]	630[e]	614(12)[f]
$R_e(a\,^3\Sigma)$	[a_0]	9.62[c]	10.28[d]		
$D_e(a\,^3\Sigma)$	[meV]	21.7(2)[c]	25.9(2)[d]		

$\mathrm{Rg}^*(\mathrm{ms}\ ^3P_2)+\mathrm{Na}(3s)$		$\mathrm{Ne}^*(3s\ ^3P_2)$	$\mathrm{Ar}^*(4s\ ^3P_2)$	$\mathrm{Kr}^*(5s\ ^3P_2)$	$\mathrm{Xe}^*(6s\ ^3P_2)$
R_e^*	[a_0]	6.1(3)	6.8(3)	7.1(3)	7.5(3)
$\hat{R}=R_e^*+\Delta R$	[a_0]	6.18(30)	7.0(3)	7.36(30)	7.84(30)
$f(\Delta R)^2/2$	[meV]	1	4	6	10
$V^+(\infty)-V^+(\hat{R})$	[meV]	28(6)[g]	74(11)[g]	88(14)[h]	108(18)[h]
E_0-E_*	[meV]	647(12)	524(12)	471(12)	437(12)
D_e^*	[meV]	676(18) 672(20)[i]	602(23)	565(26)	555(30)

$\mathrm{Rg}^*(\mathrm{ms}\ ^3P_0)+\mathrm{Na}(3s)$		$\mathrm{Ne}^*(3s\ ^3P_0)$	$\mathrm{Ar}^*(4s\ ^3P_0)$	$\mathrm{Kr}^*(5s\ ^3P_0)$	$\mathrm{Xe}^*(6s\ ^3P_0)$
R_e^*	[a_0]	9.5(1.0)	9.0(1.0)	7.8(5)	7.6(4)
$\hat{R}=R_e^*+\Delta R$	[a_0]	9.5(1.0)	9.0(1.0)	8.0(6)	7.9(6)
$f(\Delta R)^2/2$	[meV]	–	–	3(3)	9(4)
$V^+(\infty)-V^+(\hat{R})$	[meV]	5(3)[g]	25(17)[g]	62(24)[h]	106(38)[h]
E_0-E_*	[meV]	46(16)	82(12)	367(12)	415(12)
D_e^*	[meV]	51(19) 47(18)[i]	107(25)	432(36)	530(50)

[a] Ref. 37; [b] Ref. 38; [c] Ref. 39; [d] Ref. 40; [e] Ref. 41; [f] Ref. 42; [g] Ref. 34; [h] Ref. 35; [i] Ref. 7

Previous electron spectrometric determinations of D_e^* for $\mathrm{Ne}^*(3s\ ^3P_2,\ ^3P_0)+\mathrm{Na}(3s)$ by Lorenzen et al. [7] are in good agreement with the present results. For $\mathrm{Ar}^*(^3P_{2,0})+\mathrm{Na}(3s)$, an estimate of the (effective) well depth D_e^* was obtained by Neynaber and Magnuson [36] from an analysis of the ion kinetic energies in a merged-beams experiment. The metastable Ar* beam was not state-selected, and the $\mathrm{Ar}^*(^3P_2)/\mathrm{Ar}^*(^3P_0)$ flux ratio was not known; therefore, their estimate $D_e^*[\mathrm{Ar}^*+\mathrm{Na}]=(0.3\text{–}0.4)$ eV [36] cannot be easily compared with our state-resolved electron spectrometric results.

4. Conclusions

We have presented well-resolved electron energy spectra for the eight Penning ionization systems $\mathrm{Rg}^*(\mathrm{ms}\ ^3P_2)+\mathrm{Na}(3s)$, $\mathrm{Rg}^*(\mathrm{ms}\ ^3P_0)+\mathrm{Na}(3s)$ (Rg=Ne, Ar, Kr, Xe; $m=3$–6). For $\mathrm{Rg}^*(^3P_2)+\mathrm{Na}(3s)$, the spectra are quite similar for the different rare gases, both in width and shape, and are dominated by an Airy peak structure at low energies. They reflect chemical type attractive interactions in the entrance channel with well depths, which decrease slowly from Rg=Ne ($D_e^*=676$ meV) to Rg=Xe ($D_e^*=555$ meV) and which amount to about 90% of the well depth for the analogous alkali-Na(3s)($X\,^1\Sigma$) systems. For $\mathrm{Rg}^*(^3P_0)+\mathrm{Na}(3s)$, the spectra vary strongly with the rare gas indicating a change in the character of the interaction from van der Waals type attraction (Ne) to chemical binding for Kr and Xe. These findings are explained on the basis of model calculations of the respective potential curves; they take into account the exchange and spin orbit interaction in the excited rare gas and the molecular interaction between the two valence s-electrons in terms of suitably chosen singlet and triplet potentials.

The model calculations also account qualitatively for the experimental finding that the ratio q_2/q_0 of the ionization cross sections for $\mathrm{Rg}^*(^3P_2)+\mathrm{Na}(3s)$ and $\mathrm{Rg}^*(^3P_0)+\mathrm{Na}(3s)$ varies strongly with the rare gas from a value around 15 for Ne to values around 1.5 for Kr and Xe. The calculations show that – apart from the mentioned differences in the respective potential curves – there are substantial differences between the $\mathrm{Rg}^*(^3P_0)+\mathrm{Na}(3s)$ systems with respect to the spin composition: in the range of internuclear distances, where ionization mainly occurs, only the $\mathrm{Ne}^*(^3P_0)+\mathrm{Na}(3s)$ system has predominantly ($\approx$90%) quartet spin symmetry, for which ionization is forbidden, since the final state $\mathrm{Rg}(^1S_0)+\mathrm{Na}^+(^1S_0)+e^-$ has doublet spin symmetry.

In the near future we plan to carry out model calculations of the electron energy distributions in order to understand the different shapes of the spectra, which are in part rather peculiar (especially the $\mathrm{Kr}^*(^3P_0)+\mathrm{Na}$ and the $\mathrm{Xe}^*(^3P_0)+\mathrm{Na}$ spectra), and in order to obtain some information on the respective autoionization width functions.

This work was supported by the Deutsche Forschungsgemeinschaft through Sonderforschungsbereich 91. We are grateful to J.P. Toennies for providing the $KrNa^+$ and $XeNa^+$ potentials [35] and to W. Müller and W. Meyer for communicating the results of their ab initio calculation for RbNa. We thank W. Demtröder for a useful discussion on alkali-Na potential data, W. Simon for experimental help, and K. Zinsmeister for technical support. We acknowledge I. Wollscheid for her help with the figures and A. Groß for her care with the manuscript.

References

1. Hotop, H., Niehaus, A.: Z. Phys **238**, 452 (1970)
2. Hotop, H.: In: Electronic and atomic collisions. Oda, N., Takayanagi, K. (eds.), p. 271f. Amsterdam: North Holland Publ. Co. 1980
3. Niehaus, A.: Adv. Chem. Phys. **45**, 399 (1981); Phys. Rep. **186**, 149 (1990)
4. Yencha, A.J.: Electron Spectrosc. **5**, 197 (1984)
5. Morgner, H., Niehaus, A.: J. Phys. B **12**, 1805 (1979)
6. Lorenzen, J., Morgner, H., Bußert, W., Ruf, M.-W., Hotop, H.: Z. Phys. A – Atoms and Nuclei **310**, 141 (1983)
7. Lorenzen, J., Hotop, H., Ruf, M.-W.: Z. Phys. D – Atoms, Molecules and Clusters **1**, 261 (1986)
8. Ruf, M.-W., Yencha, A.J., Hotop, H.: Z. Phys. D – Atoms, Molecules and Clusters **5**, 9 (1987)
9. Müller, M.W. Bußert, W., Ruf, M.-W., Hotop, H., Meyer, W.: Phys. Rev. Lett. **59**, 2279 (1987)
10. Waibel, H., Ruf, M.-W., Hotop, H.: Z. Phys. D – Atoms, Molecules and Clusters **9**, 191 (1988)
11. Merz, A., Müller, M.W., Ruf, M.-W., Hotop, H., Meyer, W., Movre, M.: Chem. Phys. Lett. **160**, 377 (1989)
12. Padial, N.T., Cohen, J.S., Martin, R.L., Lane, N.F.: Phys. Rev. A **40**, 117 (1989)
13. Merz, A., Müller, M.W., Ruf, M.-W., Hotop, H., Meyer, W., Movre, M.: Chem. Phys. **144** (1990) (in press)
14. Meyer, W., Movre, M.: Z. Phys. D – Atoms, Molecules and Clusters (to be published)
15. Hotop, H., Lorenzen, J., Zastrow, A.: J. Electron Spectrosc. Relat. Phenom. **23**, 347 (1981)
16. Dagdigian, P.J., Campbell, M.L.: Chem. Revs. **87**, 1 (1987)
17. Sadeghi, N., Cheaib, M., Setser, D.W.: J. Chem. Phys. **90**, 219 (1989)
18. Edqvist, O., Lindholm, E., Selin, L.E., Sjögren, H., Åsbrink, L.: Ark. Fys. **40**, 439 (1970)
19. Natalis, P., Collin, J.E., Delwiche, J., Caprace, G., Hubin, M.-J.: J. Electron Spectrosc. Relat. Phenom. **17**, 421 (1979)
20. Meijer, H.A.J.: Thesis, Rijksuniversiteit Utrecht, 1988 (available on request)
21. Treibel, K.: Diplomarbeit, Univ. Kaiserslautern, 1982 (unpublished)
22. Kraft, T., Ruf, M.-W., Hotop, H.: Z. Phys. D – Atoms, Molecules and Clusters **14**, 179 (1989)
23. Weissmann, G., Ganz, J., Siegel, A., Waibel, H., Hotop, H.: Opt. Commun. **49**, 335 (1984)
24. Sadeghi, N., Sabbagh, J.: Phys. Rev. A **16**, 2336 (1977)
25. Hotop, H., Klar, D., Kraft, T., Ruf, M.-W., Schmitz, U., Simon, W.: XVI ICPEAC, New York, Abstracts of Contributed Papers. Dalgarno, A., Freund, R.S., Lubell, M.S., Lucatorto, T.B. (eds), p. 774 (1989)
26. Setser, D.W., Dreiling, T.D., Brashears, Jr., H.C., Kolts, J.H.: Faraday Disc. Chem. Soc. **67**, 255 (1979)
27. Haberland, H., Lee, Y.T., Siska, P.E.: Adv. Chem. Phys. **45**, 487 (1981)
28. Bußert, W., Bregel, T., Ganz, J., Harth, K., Siegel, A., Ruf, M.-W., Hotop, H., Morgner, H.: J. Phys. (Paris) **46**, C1–199 (1985)
29. Schmidt, I.: Dissertation, Univ. Kaiserslautern, 1989 (unpublished); Schmidt, I., Müller, W., Meyer, W.: Chem. Phys. (submitted for publication)
30. Hotop, H., Niehaus, A.: Z. Phys. **228**, 68 (1969)
31. Morgner, H.: Comments At. Mol. Phys. **21**, 195 (1988)
32. Miller, W.H.: J. Chem. Phys. **52**, 3563 (1970)
33. Miller, T.M., Bederson, B.: Adv. At. Mol. Phys. **13**, 1 (1978)
34. Ahlrichs, B., Böhm, H.J., Brode, S., Tang, K.T., Toennies, J.P.: J. Chem. Phys. **88**, 6290 (1988)
35. Toennies, J.P.: Private communication (1989)
36. Neynaber, R.H., Magnuson, G.D.: J. Chem. Phys. **67**, 430 (1977)
37. Kusch, P., Hessel, M.M.: J. Chem. Phys. **68**, 2591 (1978)
38. Barrow, R.F., Vergès, J., Effantin, C., Hussein, K., d'Incan, J.: Chem. Phys. Lett. **104**, 179 (1984)
39. Li, Li, Rice, S.F., Field, R.W: J. Chem. Phys. **82**, 1178 (1985)
40. Ross, A.J., Effantin, C., d'Incan, J., Barrow, R.F.: Mol. Phys. **56**, 902 (1985)
41. Müller, W., Meyer, W.: Private communication of ab initio results
42. Diemer, U., Weickenmeier, H., Wahl, M., Demtröder, W.: Chem. Phys. Lett. **104**, 489 (1984)